Molecular Pharmacology Fast Forward. Published on October 1, 2015 as DOI: 10.1124/mol.115.100784
This article has not been copyedited and formatted. The final version may differ from this version.

Rational engineering defines a molecular switch that is essential for activity of spider-venom peptides against the analgesics target $Na_V1.7$

Julie K. Klint, Yanni K.-Y. Chin, and Mehdi Mobli

Institute for Molecular Bioscience, The University of Queensland, St. Lucia, QLD 4072, Australia (J.K.K., Y.K.Y.C); Centre for Advanced Imaging, The University of Queensland, St. Lucia, QLD 4072, Australia (M.M)

Molecular Pharmacology Fast Forward. Published on October 1, 2015 as DOI: 10.1124/mol.115.100784
This article has not been copyedited and formatted. The final version may differ from this version.

Running title: An essential switch for peptide inhibition of $Na_V1.7$

Dr Mehdi Mobli:

Phone: +61 7 334 60352

Fax: +61 7 3365 3833

Email: m.mobli@uq.edu.au

Number of text pages: 29

Number of tables: 2

Number of figures: 5

Number references: 31

Number of words in abstract: 242

Number of words in introduction: 682

Number of words in discussion: 1500

Abbreviations: Na_V, voltage-gated sodium channel; hNa_V 1.7, human voltage-gated sodium channel subtype 1.7; K_V, voltage-gated potassium channel; WT, wild type; CHO, Chinese hamster ovary; PCR, polymerase chain reaction; BSA, HPLC, high performance liquid chromatography; MBP, bovine serum albumin; maltose binding protein; MALDI, matrix-assisted laser desorption/ionization; TOF, time of flight; MS, mass spectrometry; RP, reverse phase; TEV, tobacco etch virus; TFA, trifluoroacetic acid; NOE, nuclear overhauser effect; ICK, inhibitor cystine knot; POPG, 1-palmitoyl-2-oleoyl-*sn*-glycero-3-phospho-(1'-*rac*-glycerol) ; POPC,1-palmitoyl-2-oleoyl-*sn*-glycero-3-phosphocholine; LMV, large multilamellar vesicles; LUV, large unilamellar lipid vesicles

Molecular Pharmacology Fast Forward. Published on October 1, 2015 as DOI: 10.1124/mol.115.100784
This article has not been copyedited and formatted. The final version may differ from this version.

Abstract

Many spider venom-peptides are known to modulate the activity of the voltage-gated sodium channel $Na_V1.7$, which has emerged as a promising analgesic target. A class of spider venom-peptides (NaSpTx1) in particular have been found to potently inhibit $Na_V1.7$ (nanomolar IC_{50}), and shown to produce analgesic effects in animals. However, one member of this family, μ-TRTX-Hhn2b (Hhn2b), does not inhibit mammalian Na_V channels expressed in dorsal root ganglia at concentrations up to 100 μM. This peptide is classified as a NaSpTx1 member by virtue of its cysteine spacing and sequence conservation over functionally important residues. Here, we have performed detailed structural and functional analyses of Hhn2b leading us to identify two non-pharmacophore residues that contribute to $hNa_V1.7$ inhibition by non-overlapping mechanisms. These findings allowed us to produce a double mutant of Hhn2b that shows nanomolar inhibition of $hNa_V1.7$. Traditional structure/function analysis did not provide sufficient resolution to identify the mechanism underlying the observed gain of function. However, by solving the high-resolution structure of both the wild type and mutant peptides using advanced multidimensional NMR experiments, we were able to uncover a previously unknown network of interactions that stabilize the pharmacophore region of this class of venom-peptides. We further monitored the lipid binding properties of the peptides and identified that one of the key amino acid substitutions also selectively modulates the binding of the peptide to anionic lipids. These results will further aid the development of peptide-based analgesics for the treatment of chronic pain.

Molecular Pharmacology Fast Forward. Published on October 1, 2015 as DOI: 10.1124/mol.115.100784
This article has not been copyedited and formatted. The final version may differ from this version.

Introduction

Voltage-gated sodium (Na_V) channels are transmembrane proteins that are essential for the initiation and propagation of action potentials in excitable cells. Na_V channels are classified into nine different subtypes denoted $Na_V1.1$ to $Na_V1.9$ (Catterall et al., 2005). In recent years, $Na_V1.7$ has emerged as a validated pain target based on several human genetic studies. Gain-of-function mutations in the *SNC9A* gene encoding the pore-forming α-subunit of $Na_V1.7$, have been shown to cause painful inherited neuropathies (Cheng et al., 2011; Dabby et al., 2010; Estacion et al., 2008; Theile et al., 2011; Yang et al., 2004) whereas loss-of-function mutations in *SCN9A* result in a congenital indifference to all forms of pain (Cox et al., 2006). This suggests that subtype-selective inhibitors of $Na_V1.7$ are likely to be useful analgesics for treating a broad range of pain conditions (England and Rawson, 2010).

Many venomous animals have evolved venom-peptides that modulate the activity of Na_V channels. Spider venoms in particular are rich in Na_V channel modulators, with one third of all known ion channel venom-peptides from spider venoms acting on Na_V channels (Klint et al., 2012). Based on their primary structure and cysteine scaffold, these venom-peptides can be classified into 12 distinct families of spider venom-peptides that modulate the activity of Na_V channels (NaSpTxs) (Klint et al., 2012).

Members of the NaSpTx1 family of spider venom-peptides have been shown to potently inhibit $Na_V1.7$ (nanomolar IC_{50}), with the best-studied peptide from this family being Huwentoxin IV (μ-TRTX-Hh2a, hereon referred to as Hh2a) (Peng et al., 2002). However, one member of this family, Hainantoxin I (μ-TRTX-Hhn2b, hereon referred to as Hhn2b) isolated from *H. hainana* shows no inhibition of TTX-sensitive or TTX-resistant Na_V channels expressed in dorsal root ganglia (DRGs) at

Molecular Pharmacology Fast Forward. Published on October 1, 2015 as DOI: 10.1124/mol.115.100784
This article has not been copyedited and formatted. The final version may differ from this version.

concentrations up to 100 μM (Li et al., 2003). Hhn2b was subsequently further tested against individual Na_V channel subtypes expressed in *X. leavis* oocytes. Hhn2b displayed weak inhibition of $Na_V1.2$ (IC_{50} 68 μM) and more potent (but still weak) inhibition of the insect neuronal Na_V channel, para/tipE (IC_{50} 4.3 μM), with no effect on $Na_V1.4$ and $Na_V1.5$ up to 100 μM (Li et al., 2003). Thus, this venom-peptide consistently lacks potency against mammalian Na_V channels.

Understanding the molecular basis of the peptide-channel interaction is essential for the rational development of venom-based analgesics. Thus, to explore the unexpected paucity in channel inhibition by the NaSpTx1 peptide Hhn2b, we have here recombinantly produced isotope labelled ($^{13}C/^{15}N$) Hhn2b in a heterologous expression system, allowing us to determine its high-resolution structure by multidimensional NMR spectroscopy. Consistent with the classification of Hhn2b as a NaSpTx1 member and its sequence identity over amino acid residues that are known to be key determinants for Na_V inhibition (Fig. 1) (Klint et al., 2012; Liu et al., 2012; Minassian et al., 2013; Revell et al., 2013), we also found the overall fold of Hhn2b to be in close agreement with other members of the NaSpTx1 family. Based on the 3D structure and sequence alignment of NaSpTx1 venom-peptides, we identified several possible amino acids in Hhn2b that may explain the conspicuous lack of activity of the peptide. Using our recombinant expression system we were able to introduce mutations at the amino acids putatively identified as functionally important. Two of the mutations (G7W and N24S) resulted in a gain of $Na_V1.7$ activity, and remarkably, simultaneous mutation of both these residues resulted in a double mutant that showed nanomolar inhibition of $Na_V1.7$. The high-resolution solution structure of this double mutant was also determined using high-resolution NMR spectroscopy and detailed analyses showed that the mutations cause subtle displacements of the sidechains of

Molecular Pharmacology Fast Forward. Published on October 1, 2015 as DOI: 10.1124/mol.115.100784
This article has not been copyedited and formatted. The final version may differ from this version.

key pharmacophore residues, thus indirectly perturbing the pharmacophore of the peptide. Further NMR studies of the binding of the peptides to liposomes showed that Hhn2b does not bind strongly to lipids whilst the G7W/N24S-Hhn2b binds selectively to anionic lipid bilayers. We further show that the G7W mutation alone accounts for this gain of lipid binding. Together these results provide novel insight into the structural determinants of Na_V channel inhibition by NaSpTx1 venom peptides and provide new avenues for fine-tuning of activity and lipid binding through subtle sequence variation.

Materials and Methods

Expression vector and mutagenesis. A synthetic gene facilitating periplasmic expression (GeneArt, Invitrogen, Regensburg, Germany) encoding Hhn2b was used as previously described (Klint et al., 2013). Site-directed mutagenesis was performed by quick-change PCR method using standard protocols with Platinum Pfx DNA Polymerase (Invitrogen) (Qi and Scholthof, 2008). Mutant cDNA constructs were sequenced to verify the desired mutation and the absence of unwanted spontaneous mutations (AGRF, Brisbane, Australia) before transformation into *E. coli* (BL21(λDE3)).

Production of Recombinant WT Hhn2b and mutants. Peptides were produced following an optimized protocol described previously (Klint et al., 2013). Peptide purity was assessed by analytical HPLC and MALDI-TOF mass spectrometry and all peptides used showed >95% purity.

Two-electrode voltage-clamp recording from X. laevis oocytes. Human Na_V subtypes (co-injected with human β1 subunit) constructs were expressed in *X. laevis* oocytes.

Molecular Pharmacology Fast Forward. Published on October 1, 2015 as DOI: 10.1124/mol.115.100784
This article has not been copyedited and formatted. The final version may differ from this version.

Two-electrode voltage-clamp recording techniques (OC-725C, Warner Instruments; 150-µl recording chamber) were used to measure Na^+ currents 1–4 days after cRNA injection and incubation at 17°C in ND96 that contained (in mM): 96 NaCl, 2 KCl, 5 HEPES, 1 $MgCl_2$ and 1.8 $CaCl_2$, 50 µg/ml gentamycin, pH 7.6. Data were filtered at 4 kHz and digitized at 20 kHz using pClamp software (Axon). Microelectrode resistances were 0.1–1 MΩ when filled with 3 M KCl. The external recording solution contained (in mM): 96 NaCl, 2 KCl, 5 HEPES, 1 $MgCl_2$ and 1.8 $CaCl_2$, pH 7.6 with NaOH. All experiments were performed at RT (~22 °C) and peptide samples were diluted in recording solution with 0.1% BSA. Leak and background conductances, identified by blocking the channel with TTX, were subtracted for all Na_V currents. All chemicals were obtained from Sigma-Aldrich.

Off-line data analysis was performed using Clampfit (Axon), Origin 7.5 (Originlab), and Microsoft Solver (Microsoft Excel).

Automated patch-clamp. Human $Na_V1.7$ EZcells™ division-arrested cells were obtained from ChanTest (Cleveland, Ohio, USA, Lot #1543).

Na^+ currents were measured using the automated electrophysiology platform QPatch™ 16x (Sophion, Denmark) in single-hole configuration. Extra cellular Ringers solution (in mM): 1 $CaCl_2$, 1 $MgCl_2$, 5 HEPES, 3 KCl, 140 NaCl, 0.1 $CdCl_2$, 20 TEA-Cl, pH 7.3 (NaOH), 320 mOsm and intra cellular Ringers solution (in mM): 140 CsF, 1/5 EGTA/CsOH, 10 HEPES, 10 NaCl. pH 7.3 (NaOH), 320 mOsm. Cells positioned on the chip using a positioning pressure of –100 mbar. Gigaseals were obtained by applying negative pressure to the cells between –20 and –130 mbar for 4 min at a membrane holding potential of –90 mV. Whole cell configuration was obtained by 1 s suction pulses of increasing intensity from –250 mbar to –500 mbar in

Molecular Pharmacology Fast Forward. Published on October 1, 2015 as DOI: 10.1124/mol.115.100784
This article has not been copyedited and formatted. The final version may differ from this version.

50 mbar increments with 10 s between pulses. Whole cell configuration was confirmed by development of a capacitative transient >4 pF.

For measuring $Na_V1.7$ currents, the membrane potential was held at –80 mV then stepped to –120 mV for 100 ms to remove any potential fast inactivated channels, followed by a step to 0 mV for 10 ms to activate $Na_V1.7$. The membrane potential was held at –80 mV between sweeps. Hhn2b and mutants were dissolved in extracellular solution with 0.1% BSA (fatty acid free) and after obtaining baseline recordings, 5 µL was applied and the effect was assessed after 1 min peptide incubation with the channel by applying the voltage protocol 25 times at 5 s intervals, to ensure steady-state inhibition was reached. Data were sampled at 10 kHz and filtered using a 4 pole Bessel filter at 3 kHz. Series resistance was compensated 75%. Off-line data analysis was performed using Qpatch assay software v5.0 (Sophion, Denmark) and Microsoft Excel (for Mac 2011, version 14.3.4). Peak inward current at 0 mV was normalized to cell capacitance (pA/pF) steady state current density in response to each sample concentration was normalized to vehicle control (EC + 0.1% BSA) and plotted as fractional current. Fraction of inhibition was obtained using Prism 6 (Graphpad software) by column statistics and is given as the mean fraction of inhibition and the standard deviation. IC_{50} values were obtained by non-linier fit also by Prism 6 using the equation: Y=Bottom + (Top – Bottom)/1+10^(Log(IC_{50} – x)* HillSlope)). The significance of the difference in inhibition of $Na_V1.7$ currents by different peptides was calculated by an unpaired t-test using Prism 6 (Graphpad software). This comparison was only done between peptides that showed inhibition at 1 µM. Peptides showing no inhibition at 1 µM were not included in the t-test as much higher (> 1 µM) peptide concentrations would be required to produce measurable inhibition.

Molecular Pharmacology Fast Forward. Published on October 1, 2015 as DOI: 10.1124/mol.115.100784
This article has not been copyedited and formatted. The final version may differ from this version.

NMR structure determination of WT and G7W/N24S Hhn2b. The structure of WT and G7W/N24S mutants of Hhn2b were determined using heteronuclear NMR. Both samples contained 300 μL of $^{13}C/^{15}N$-labeled peptides at 300 μM in 20 mM sodium acetate solution with 5% D_2O at pH 5. All spectra were acquired at 298 K on a Bruker Avance II+ 900 MHz spectrometer equipped with a cryogenically cooled triple resonance probe. Resonance assignments were obtained using 2D ^{1}H-^{15}N-HSQC, 2D ^{1}H-^{13}C-HSQC, 3D HNCACB, 3D CBCA(CO)NH, 3D HNCO, 3D HBHA(CO)NH and 4D HCC(CO)NH-TOCSY spectra, in which the 3D and 4D spectra were acquired using non-uniform sampling and transformed using maximum entropy reconstruction with the Rowland NMR Toolkit (http://www.rowland.org/rnmrtk/toolkit.html) as described previously (Mobli et al., 2007). Inter-proton distance restraints were obtained from 3D ^{13}C-aliphatic, ^{13}C-aromatic and ^{15}N NOESY-HSQC spectra acquired using a mixing time of 200 ms. Spectra were analysed using CcpNmr Analysis 2.4.1 (Vranken et al., 2005). Dihedral angle restraints were derived from Talos^{+} protein backbone dihedral angle prediction program (Shen et al., 2009), with the restraints range for structure calculations set to twice the estimated standard deviation. The NOESY spectra were manually peak picked and the torsion angle dynamics package CYANA3 (Guntert, 2004) was then used to automatically assign the peak lists, extract distance restraints and calculate an ensemble of structures. 200 structures were calculated for each peptide and the top 30 were selected based on the final CYANA target function value and ranked based on their stereochemical quality as judged by MolProbity (Chen et al., 2010).

Preparation of POPG and POPC liposomes. Stock solution of 1-palmitoyl-2-oleoyl-*sn*-glycero-3-phospho-(1'-*rac*-glycerol) (POPG; 25 mg/mL) or 1-palmitoyl-2-oleoyl-*sn*-glycero-3-phosphocholine (POPC; 25 mg/mL) (Avanti) in chloroform were

Molecular Pharmacology Fast Forward. Published on October 1, 2015 as DOI: 10.1124/mol.115.100784
This article has not been copyedited and formatted. The final version may differ from this version.

dried down under nitrogen gas and left under vacuum overnight. The dried film of lipid was rehydrated in 50 mM sodium acetate, pH 5, 50 mM NaCl and 5% D_2O by shaking the mixture at room temperature for 1 hour. The hydration yielded large, multilamellar vesicles (LMV). To downsize the LMV to homogenous, large unilamellar lipid vesicles (LUV), the suspension was freeze-thawed repeatedly for 20 times, followed by extruding it through a filter with pore size of 100 nM (Avanti) for 21 times.

NMR titrations of liposomes to Hhn2b peptides. Prepared liposome solutions or buffer solution was added directly to the lyophilised peptide. Each sample contained 50 μM of peptide in 50 mM sodium acetate, 50 mM NaCl and 5% D_2O, pH 5, with either no liposomes, 1.5 mM POPG or 1.5 mM of POPC. The sample volume was 160 μL and it was contained and run in a 3 mm NMR tube (Norelle, Marion NC, USA). Spectra were recorded at 298 K on a Bruker Avance II+ 900 MHz spectrometer equipped with a cryogenically cooled triple resonance probe. Spectra were processed and analysed using Topspin (Bruker).

Results

Effect of recombinant Hhn2b on human Na_V channel subtypes expressed in oocytes. Peptide expression, purity and identity were assessed by SDS-PAGE, HPLC and mass spectrometry (Supplemental Fig. S1). The function of the recombinantly expressed Hhn2b was initially assessed at a concentration of 1 μM against $hNa_V1.2$, $hNa_V1.5$, and $hNa_V1.7$ expressed in *X. laevis* oocytes. As can be seen from Supplemental Fig. S2, 1 μM Hhn2b inhibited $hNa_V1.2$ by 25% and had no effect on $hNa_V1.7$, $hNa_V1.3$ and $hNa_V1.5$. This is in agreement with the previously reported

Molecular Pharmacology Fast Forward. Published on October 1, 2015 as DOI: 10.1124/mol.115.100784
This article has not been copyedited and formatted. The final version may differ from this version.

potency and selectivity of the native peptide (Li et al., 2003), and indicates that the recombinant peptide has the same structural and functional characteristics as the native toxin.

Effect of wild-type and mutant Hhn2b on human $Na_V1.7$. The remaining activity assays were measured by automated patch-clamp electrophysiology against $hNa_V1.7$ stably expressed in CHO cells. The results are summarized in Fig. 2 and Table 1. In agreement with the initial assessment WT Hhn2b displays no inhibition of $hNa_V1.7$ (10 μM highest concentration tested).

Comparison of the sequence and structure of Hhn2b with other members of this toxin family identified four residues (K4/G7/N24/V32) in proximity to the proposed pharmacophore region that were not conserved in Hhn2b. K4 was mutated to a leucine to remove the positive charge, which is not present in other Na_V inhibiting members of this family. G7 was mutated to a tryptophan residue, as this position is often occupied by a residue with an aromatic sidechain. N24 was mutated to an otherwise absolutely conserved serine residue. Finally, V32, which is a conserved tyrosine residue, was mutated to a tryptophan residue as this substitution had previously been seen to improve the activity of Hh2a (Revell et al., 2013).

K4L and V32W point mutations did not result in any gain of activity against $hNa_V1.7$ (Fig. 2B). Point mutations of G7W and N24S on the other hand, each resulted in a gain of activity against $hNa_V1.7$ with IC_{50}s of 2.7 ± 0.4 μM and 4.0 ± 0.5 μM respectively. Combining these two mutations in a double mutant, G7W/N24S Hhn2b resulted in potent inhibition of $hNa_V1.7$, with an IC_{50} of 440 ± 4 nM (Fig. 2C).

To test whether the gain in activity of the N24S mutation resulted from the removal of an unfavorable interaction by the asparagine residue with the channel, a G7W/N24A

Molecular Pharmacology Fast Forward. Published on October 1, 2015 as DOI: 10.1124/mol.115.100784
This article has not been copyedited and formatted. The final version may differ from this version.

mutant was also generated. This mutant showed a similar affinity as the G7W mutation alone (IC_{50} of 8.6 ± 1.7 μM), suggesting that the gain in activity is due to a specific effect of the serine residue.

Finally we found that it is possible to remove the inhibitory effect of the G7W/N24S Hhn2b double mutant by mutating the essential Trp29 residue to an alanine (no inhibition at 10 μM). This position has previously also been shown to be critical in the activity of Hh2a (Revell et al., 2013). We further found that a substitution of Trp29 to a less bulky aromatic residue was tolerated but reduced potency, with the triple mutant G7W/N24S/W29F Hhn2b resulting in an IC_{50} of 1.0 ± 0.2 μM.

Structural characterization of WT and G7W/N24S Hhn2b. Uniformly $^{13}C/^{15}N$-labelled WT and G7W/N24S mutant of Hhn2b were produced for structural studies by NMR. $^{1}H_N$, ^{15}N, $^{13}C'$, $^{13}C\alpha$, $^{13}C\beta$ resonance assignments for both peptides were obtained by standard triple resonance experiments and a 4D HCC(CO)NH-TOCSY experiment that provides sidechain ^{1}H-^{13}C connectivities (Mobli et al., 2010). Complete chemical shift assignments were deposited to the BioMagResBank. The accession numbers for the WT and G7W/N24S mutant Hhn2b are 25031 and 25421 respectively.

The automated NOE assignment procedure of CYANA 3.0 was used, and the program assigned 96.2% and 95.1% of all NOESY cross-peaks of WT and G7W/N24S mutant of Hhn2b, respectively. The final structures were calculated using 446 unique distance restraints for the WT structure and 437 for the G7W/N24S mutant. Atomic coordinates for the final ensembles were deposited in the Protein Data Bank. The PDB ID for the WT and G7W/N24S Hhn2b are 2MQF and 2MXO respectively. Statistics highlighting the high precision and stereochemical quality of the ensembles are listed in Table 2. Both structural ensembles are highly precise with

the backbone and heavy-atom r.m.s.d. of the WT Hhn2b over the structurally ordered region (residue 3-32) found to be 0.17 Å ± 0.05 and 0.63 Å ± 0.13, respectively, and the backbone and heavy-atom r.m.s.d. of the structural ensemble of G7W/N24S mutant over the same region are 0.14 Å ± 0.04 and 1.18 Å ± 0.27, respectively.

As a member of the NaSpTx1 family, Hhn2b is expected to adopt the inhibitor cystine knot (ICK) motif, with disulfide connectivities between cysteine residues 1–4, 2–5 and 3–6 (by order in the amino acid sequence). The disulfide connectivity of the WT and G7W/N24S Hhn2b was determined from the preliminary structures calculated without disulfide bond restraints. In both peptides, disulfide linkages were formed between Cys3 and Cys18, Cys10 and Cys23 and between Cys17 and Cys30, hence confirming that the peptide adopts the ICK motif. The structure contains an anti-parallel beta hairpin loop and a hydrophobic face, comprised of several hydrophobic residues that are highly conserved among venom-peptides in this family (Phe6, Tyr21, Trp29, Val32 in Hhn2b).

The high-resolution structures of the inactive WT Hhn2b and the most potent mutant (G7W/N24S) allowed direct structural comparison of the two peptides. As illustrated in the overlay of the two structures in Fig. 3, the overall structure of Hhn2b remains similar upon the substitution of Gly7 and Asn24. In the absence of 3D structural data the fold of the peptides can also be evaluated based on backbone chemical shifts, which are sensitive to changes in the secondary structure. Typically H_α shifts or overlay of ^{15}N HSQC spectra are used, both of which also showed that the G7W/N24S mutant retained a similar fold as the WT Hhn2b (see Fig. 4 and Supplemental Fig. S3).

The structural differences between the two peptides, however, lie in subtle changes of the sidechain orientation of certain residues. In contrast to the well-defined aromatic

Molecular Pharmacology Fast Forward. Published on October 1, 2015 as DOI: 10.1124/mol.115.100784
This article has not been copyedited and formatted. The final version may differ from this version.

cluster at the hydrophobic surface (Phe6, Tyr21, Trp29), the introduced tryptophan residue at position 7 (G7W) in the mutant was found to have no inter-residue NOEs, hence this sidechain does not adopt an ordered orientation and is likely disordered in solution (Fig. 3A). The high flexibility of the Trp7 side chain is partly responsible for the higher heavy atom r.m.s.d. of the mutant structure as compared to the WT.

Overlaying the structures of the WT and the G7W/N24S Hhn2b also revealed a subtle displacement of the Trp29 residue in the mutant (Fig. 3C). While the aromatic ring of the Trp29 in the WT structure is pointing away from Asp27, Trp29 in the G7W/N24S mutant is tilted and is in closer proximity to Asp27. The repositioning of Trp29 is also consistent with the unusual chemical shifts observed for the atoms of Asp27 in the mutant compared to the wild type Hhn2b. Aromatic rings are known to exert ring currents that would account for the observed change in the chemical shift. To quantify the significance of the observed chemical shift changes, we measured the chemical shift differences ($\Delta\delta$) of all non-mutated atoms of the WT and G7W/N24S Hhn2b (Fig. 4). These results show that Asp27 indeed displays the largest chemical shift perturbations. By comparing the ^{15}N-HSQC and the 2D NOESY spectra of the N24S mutant with those from the WT and G7W/N24S Hhn2b we were able to see that the change in the chemical shifts in Asp27 occurs with the introduction of Ser24 and is further enhanced by introduction of Trp7 (Supplemental Fig. S3 and S4), indicating that both residues contribute to this reorientation.

The second cluster of $\Delta\delta$ outliers include the HE1 and CD1 atoms from the sidechain indole ring of Trp29, and smaller yet consistent changes in the chemical shift of the sidechain atoms of Lys31 (Fig. 4). In particular we note that the largest changes in the chemical shifts of Lys31 are near the charged amino group of the sidechain. The charged group would exert a large electric field component that would significantly

Molecular Pharmacology Fast Forward. Published on October 1, 2015 as DOI: 10.1124/mol.115.100784
This article has not been copyedited and formatted. The final version may differ from this version.

affect the chemical shift of nearby atoms, consistent with the changes of chemical shift seen for HE1 and CD1 of Trp29. In the structural overlay we indeed see a change in the orientation of the sidechain of Lys31, which appears to move towards Ser24 and the indole ring of Trp29. Thus, the subtle change in the structure appears to be consistent with chemical shift differences observed. We note that the large shift in HE1 of Trp29 is present in the G7W and the G7W/N24S mutants but not in the N24S mutant, suggesting that the rearrangement of Lys31 is not strongly dependent on Ser24, and largely dictated by the introduction of Trp7.

Interactions of Hhn2b and mutants with liposomes. 1D ^{1}H-NMR spectra were acquired for the WT, G7W, N24S and G7W/N24S mutants of Hhn2b in the presence and absence of anionic POPG or neutral POPC liposomes. In the absence of liposomes, all peptides displayed a well-dispersed ^{1}H spectrum, consistent with the globular fold of the peptides. The NH region (~6-11 ppm) was monitored, where signals from the buffer and lipids do not interfere with those of the peptide. In the presence of POPC and POPG, the ^{1}H spectra of the WT and N24S mutants show well-resolved and sharp line shapes (Fig. 5 and Supplemental Fig. S5). This shows that the molecules retain a fast molecular correlation time, indicating that they do not associate strongly with the much larger liposomes. Similarly the G7W and G7W/N24S mutants showed no significant change in their ^{1}H spectra in the presence of POPC liposomes, whilst in contrast the presence of POPG resulted in extensive linebroadening (Fig. 5), indicating that the Trp7 containing peptides were bound to the liposomes. These results clearly show that the G7W and G7W/N24S mutants interact with the POPG liposomes with much higher affinity than the WT and N24S mutant.

Molecular Pharmacology Fast Forward. Published on October 1, 2015 as DOI: 10.1124/mol.115.100784
This article has not been copyedited and formatted. The final version may differ from this version.

Discussion

Switching on Nav1.7 activity: In this study we have investigated the structural basis of the conspicuous lack of activity exhibited by the spider venom peptide Hhn2b. This peptide has based on sequence identity and intercysteine spacing been classified as part of a family of spider venom peptides that includes several members known to potently inhibit $Na_V1.7$, including the well characterized Hh2a venom peptide. Critically, it has been shown that the residues essential for Hh2a activity are Trp30 (Trp29 in Hhn2b) and Lys32 (Lys31 in Hhn2b). Mutation of either of these residues to alanine completely abolishes the activity of Hh2a at $Na_V1.7$. In Hhn2b both of these residues are present yet the peptide remains inactive. In order to understand the structural basis for the apparent loss of Na_V activity of Hhn2b we determined its high-resolution structure, which confirms that the overall fold of the peptides is similar to the structure of other members of this family. There were, however, a number of amino acid differences, which were found to be in close contact with the important Trp29 and Lys31 residues. Based on this, a series of single, double and triple mutants were generated to discern the functional importance of these residues. Our results indicated that the most important difference between Hhn2b and other toxins with respect to $Na_V1.7$ activity is the G7W and N24S substitutions in loops 1 and 4 respectively. Individual mutation of either of these residues led to a weakly active peptide, and a double mutant resulted in a nanomolar inhibitor of $Na_V1.7$.

A structural basis: The functional studies of the generated mutants identified the amino acids that account for the lack of Hhn2b activity against $Na_V1.7$. This, however, does not explain how the introduced substitutions switch on the observed inhibitory effect. To investigate structural changes that the mutations may have induced that can account for the gain in activity, we also determined the high-

Molecular Pharmacology Fast Forward. Published on October 1, 2015 as DOI: 10.1124/mol.115.100784
This article has not been copyedited and formatted. The final version may differ from this version.

resolution NMR structure of G7W/N24S Hhn2b. Comparison of the high-resolution structure of the mutant and the WT peptide showed that the difference in activity cannot be attributed to a change in the overall fold of the peptide. In the absence of further functional data or high-resolution structural data, it is tempting to conclude that the residues themselves are interacting with the channel. The lack of activity in the triple mutant N24S/G7W/W29A, however, suggests this is unlikely to be the case, and indeed the high-resolution structure of the N24S/G7W mutant shows that the mutations cause several interesting changes in the sidechain orientation of key pharmacophore residues (see Trp29 and Lys31 in Fig. 3).

Comparison of the two structures shows that introduction of Ser24 and Trp7 both contribute to the observed structural changes. The reorientation of the sidechain of Trp29 against Ser24 places the indole ring in close proximity to the hydroxyl group of the serine where it can form favorable electrostatic interactions. Similarly we find that the disordered Trp7 sidechain provides a steric hindrance leading to further packing of Trp29 against the tip of loop 4 (against Asp27). This reorientation further causes a change in the sidechain orientation of Lys31 towards Ser24 and Trp29 where it can form favorable cation-π interactions. The resulting "domino" effect that effectively reorients the pharmacophore of the peptide can be followed both through the NOE based 3D structure (Fig. 3) and the changes in the chemical shifts (Fig. 4).

These data are consistent with the mutations causing a change in the structure of the peptide, albeit in the sidechain and not the backbone of the peptide. Our findings highlight that great caution should be exercised in dissecting relative contributions of "structure" and "interaction" based on low resolution structural NMR data such as H_α chemical shift deviations and overlay of two dimensional ^{15}N-HSQC spectra. We find

Molecular Pharmacology Fast Forward. Published on October 1, 2015 as DOI: 10.1124/mol.115.100784
This article has not been copyedited and formatted. The final version may differ from this version.

instead that quantitative chemical shift analysis and high-resolution structural characterization are suitable for structure/function studies in this class of molecules.

Although little is known about how these peptides bind to Na_V channels, we note that our data is consistent with the docking model proposed for the binding of Hh2a to the domain II voltage sensor of $Na_V1.7$ (Minassian et al., 2013). In this model the peptide binds to a crevice formed between the four helices of the voltage sensor domain and reveals key interactions between Lys32 (Lys31 in Hhn2b) of the peptide and Glu811 on the channel, as well as a hydrophobic pocket formed in the channel crevice by Met750 and His754 which in the complex accommodates Trp30 (Trp29 in Hhn2b) and Phe6 (Trp7 in Hhn2b mutant) of the peptide. Conversely, the model proposed does not identify any significant interactions between Ser25 (Asn24 in Hhn2b) and the channel. This is consistent with our proposal that this serine residue is part of a structurally important network of intramolecular interactions.

Modulating lipid binding: The amphipathic nature of many spider toxins that bind to voltage gated ion channels, has led to studies investigating the role of lipid binding in their function (Milescu et al., 2007). It has been shown that spider toxins that act as gating modifiers can bind to lipid membranes (Milescu et al., 2009), and it has been proposed that together, the protein and lipid interactions prevent the voltage sensor from making the outward movement needed for channel activation (Jung et al., 2010; Lee and MacKinnon, 2004; Milescu et al., 2009; Milescu et al., 2007) Furthermore, it has been demonstrated that Hh2a is able to bind to the closed state of $Na_V1.7$ (Xiao et al., 2008), which agrees well with models proposing that the peptide reaches the voltage sensor while it is still embedded in the membrane, thereby blocking the outward movement of the sensor during channel activation (Henrion et al., 2012). These studies suggest that lipid interactions can be directly involved in the

mechanism of channel inhibition by venom peptides. It is, however, also known that lipid interactions can serve to increase the local concentration of ligands near membrane embedded receptors (Sykes et al., 2014), and that this itself has a significant effect on the measured affinity of such ligands. Lipid binding, therefore, appears to be a critical determinant of function that must be considered in structure/function studies of ligands that act on membrane embedded receptors.

Our results show that introducing a hydrophobic residue in loop 1 increases the affinity of Hhn2b towards POPG but not towards POPC liposomes. We note that although POPG is not present in mammalian cell membranes, the presence of other charged group in the membrane leaflet, as well as charges on the channel are likely to provide the necessary interactions in the relevant $hNa_V1.7$ environment. Since the mutation involved the introduction of a neutral hydrophobic residue it suggests that the basic nature of these peptides *together* with their hydrophobicity contributes to their overall lipid binding. An intriguing consequence of this is that these peptides appear to be marginally lipid binding, such that their association with mammalian lipid membranes (dominated by POPC/POPE) is transient in the absence of anionic components in the membrane leaflet. In the presence of anionic channel/lipid components their association with the lipid becomes significantly enhanced. In the context of venom evolution, this would appear to be a highly desirable property for injected venom component as it would allow the peptides to diffuse effectively near the lipid environment, where their target receptors are, without biding so strongly that it would limit their circulation from the site of injection. From a drug design perspective, our findings suggest that lipid binding and selectivity may be modulated through subtle modification of residues in loop 1.

Conclusions: In this study we have provided novel insight into the molecular determinants of Na_V channel inhibition by venom peptides in the NaSpTx1 family of toxins. We have introduced a series of mutations to convert an inactive venom peptide to a nanomolar $Na_V1.7$ inhibitor. Structural studies of both the native and the most potent engineered peptide allowed us to provide a structural basis for the recapitulated activity. The two mutations found to improve activity, N24S and G7W, perturb the sidechain orientation of the critical Trp29 and Lys31 residues. The importance of G7W and N24S in defining the orientation of the critical Trp29 residues was further supported by a triple mutant, G7W/N24S/W29A, which showed complete loss of activity. By performing lipid binding studies we found that the G7W mutation also increased the membrane binding propencity of the peptide. Thus, although both mutations are important for defining the pharmacophore region, the gain in activity by the introduced Trp7 residue may in addition be due to an increase in lipophilicity.

Venom peptides in this family have attracted considerable attention as analgesic leads for the treatment of chronic pain, and although our results shows that Hhn2b is a potent blocker of $Na_V1.7$ it is not expected to have improved subtype selectivity over other peptides in this family. Future studies will be focused on determining residues that are important for governing subtype selectivity. It is expected that the improved definition of functionally important residues provided here will guide these drug development efforts.

Molecular Pharmacology Fast Forward. Published on October 1, 2015 as DOI: 10.1124/mol.115.100784
This article has not been copyedited and formatted. The final version may differ from this version.

Acknowledgements

The authors are indebted to valuable discussions with Prof. Glenn King, A/Prof. Frank Bosmans and Dr Lachlan Rash as well as technical assistance by Mr Carus Lau. The NMR data were acquired in facilities operated by the Queensland NMR Network.

Authorship contribution

Participated in research design: Klint, Chin, Mobli

Conducted experiments: Klint, Chin

Performed data analysis: Klint, Chin, Mobli

Wrote the manuscript: Klint, Chin, Mobli

References

Bosmans F, Rash L, Zhu S, Diochot S, Lazdunski M, Escoubas P and Tytgat J (2006) Four novel tarantula toxins as selective modulators of voltage-gated sodium channel subtypes. *Mol Pharmacol* **69**(2): 419-429.

Catterall WA, Perez-Reyes E, Snutch TP and Striessnig J (2005) International Union of Pharmacology. XLVIII. Nomenclature and structure-function relationships of voltage-gated calcium channels. *Pharmacol Rev* **57**(4): 411-425.

Chen VB, Arendall WB, 3rd, Headd JJ, Keedy DA, Immormino RM, Kapral GJ, Murray LW, Richardson JS and Richardson DC (2010) MolProbity: all-atom structure validation for macromolecular crystallography. *Acta Crystallogr D Biol Crystallogr* **66**(Pt 1): 12-21.

Cheng X, Dib-Hajj SD, Tyrrell L, Te Morsche RH, Drenth JP and Waxman SG (2011) Deletion mutation of sodium channel $Na_V1.7$ in inherited erythromelalgia: enhanced slow inactivation modulates dorsal root ganglion neuron hyperexcitability. *Brain* **134**(Pt 7): 1972-1986.

Cox JJ, Reimann F, Nicholas AK, Thornton G, Roberts E, Springell K, Karbani G, Jafri H, Mannan J, Raashid Y, Al-Gazali L, Hamamy H, Valente EM, Gorman S, Williams R, McHale DP, Wood JN, Gribble FM and Woods CG (2006) An *SCN9A* channelopathy causes congenital inability to experience pain. *Nature* **444**(7121): 894-898.

Dabby R, Sadeh M, Gilad R, Lampl Y, Cohen S, Inbar S and Leshinsky-Silver E (2010) Chronic non-paroxysmal neuropathic pain - Novel phenotype of mutation in the sodium channel *SCN9A* gene. *J Neurol Sci* **301**(1-2): 90-92.

England S and Rawson D (2010) Isoform-selective voltage-gated Na^+ channel modulators as next-generation analgesics. *Future Med Chem* **2**(5): 775-790.

Estacion M, Dib-Hajj SD, Benke PJ, Te Morsche RH, Eastman EM, Macala LJ, Drenth JP and Waxman SG (2008) $Na_V1.7$ gain-of-function mutations as a continuum: A1632E displays physiological changes associated with erythromelalgia and paroxysmal extreme pain disorder mutations and produces symptoms of both disorders. *J Neurosci* **28**(43): 11079-11088.

Guntert P (2004) Automated NMR structure calculation with CYANA. *Methods Mol Biol* **278**: 353-378.

Henrion U, Renhorn J, Borjesson SI, Nelson EM, Schwaiger CS, Bjelkmar P, Wallner B, Lindahl E and Elinder F (2012) Tracking a complete voltage-sensor cycle with metal-ion bridges. *Proc Natl Acad Sci U S A* **109**(22): 8552-8557.

Jung HH, Jung HJ, Milescu M, Lee CW, Lee S, Lee JY, Eu YJ, Kim HH, Swartz KJ and Kim JI (2010) Structure and orientation of a voltage-sensor toxin in lipid membranes. *Biophys J* **99**(2): 638-646.

Klint JK, Senff S, Rupasinghe DB, Er SY, Herzig V, Nicholson GM and King GF (2012) Spider-venom peptides that target voltage-gated sodium channels: pharmacological tools and potential therapeutic leads. *Toxicon* **60**(4): 478-491.

Klint JK, Senff S, Saez NJ, Seshadri R, Lau HY, Bende NS, Undheim EA, Rash LD, Mobli M and King GF (2013) Production of Recombinant Disulfide-Rich Venom Peptides for Structural and Functional Analysis via Expression in the Periplasm of E. coli. *PLoS ONE* **8**(5): e63865.

Klint JK, Smith JJ, Vetter I, Rupasinghe DB, Er SY, Senff S, Herzig V, Mobli M, Lewis RJ, Bosmans F and King GF (2015) Seven novel modulators of the analgesic target $Na_V1.7$ uncovered using a high-throughput venom-based discovery approach. *Br J Pharmacol* **172**(10): 2445-2458.

Lee SY and MacKinnon R (2004) A membrane-access mechanism of ion channel inhibition by voltage sensor toxins from spider venom. *Nature* **430**(6996): 232-235.

Li D, Xiao Y, Hu W, Xie J, Bosmans F, Tytgat J and Liang S (2003) Function and solution structure of hainantoxin-I, a novel insect sodium channel inhibitor from the Chinese bird spider *Selenocosmia hainana*. *FEBS Lett* **555**(3): 616-622.

Liu Y, Li D, Wu Z, Li J, Nie D, Xiang Y and Liu Z (2012) A positively charged surface patch is important for hainantoxin-IV binding to voltage-gated sodium channels. *J Pept Sci* **18**(10): 643-649.

Milescu M, Bosmans F, Lee S, Alabi AA, Kim JI and Swartz KJ (2009) Interactions between lipids and voltage sensor paddles detected with tarantula toxins. *Nat Struct Mol Biol* **16**(10): 1080-1085.

Milescu M, Vobecky J, Roh SH, Kim SH, Jung HJ, Kim JI and Swartz KJ (2007) Tarantula toxins interact with voltage sensors within lipid membranes. *J Gen Physiol* **130**(5): 497-511.

Minassian NA, Gibbs A, Shih AY, Liu Y, Neff RA, Sutton SW, Mirzadegan T, Connor J, Fellows R, Husovsky M, Nelson S, Hunter MJ, Flinspach M and Wickenden AD (2013) Analysis of the structural and molecular basis of voltage-sensitive sodium channel inhibition by the spider toxin huwentoxin-IV (μ-TRTX-Hh2a). *J Biol Chem* **288**(31): 22707-22720.

Mobli M, Maciejewski MW, Gryk MR and Hoch JC (2007) An automated tool for maximum entropy reconstruction of biomolecular NMR spectra. *Nat Methods* **4**(6): 467-468.

Mobli M, Stern AS, Bermel W, King GF and Hoch JC (2010) A non-uniformly sampled 4D HCC(CO)NH-TOCSY experiment processed using maximum entropy for rapid protein sidechain assignment. *J Magn Reson* **204**(1): 160-164.

Peng K, Shu Q, Liu Z and Liang S (2002) Function and solution structure of huwentoxin-IV, a potent neuronal tetrodotoxin (TTX)-sensitive sodium channel antagonist from Chinese bird spider Selenocosmia huwena. *J Biol Chem* **277**(49): 47564-47571.

Qi D and Scholthof KB (2008) A one-step PCR-based method for rapid and efficient site-directed fragment deletion, insertion, and substitution mutagenesis. *J Virol Methods* **149**(1): 85-90.

Revell JD, Lund PE, Linley JE, Metcalfe J, Burmeister N, Sridharan S, Jones C, Jermutus L and Bednarek M (2013) Potency optimization of Huwentoxin-IV on hNa_V1.7: A neurotoxin TTX-S sodium-channel antagonist from the venom of the Chinese bird-eating spider *Selenocosmia huwena*. *Peptides* **44**: 40-46.

Shen Y, Delaglio F, Cornilescu G and Bax A (2009) TALOS+: a hybrid method for predicting protein backbone torsion angles from NMR chemical shifts. *J Biomol NMR* **44**(4): 213-223.

Sykes DA, Parry C, Reilly J, Wright P, Fairhurst RA and Charlton SJ (2014) Observed drug-receptor association rates are governed by membrane affinity: the importance of establishing "micro-pharmacokinetic/pharmacodynamic relationships" at the β2-adrenoceptor. *Mol Pharmacol* **85**(4): 608-617.

Theile JW, Jarecki BW, Piekarz AD and Cummins TR (2011) Nav1.7 mutations associated with paroxysmal extreme pain disorder, but not erythromelalgia, enhance Navβ4 peptide-mediated resurgent sodium currents. *J Physiol* **589**(Pt 3): 597-608.

Vranken WF, Boucher W, Stevens TJ, Fogh RH, Pajon A, Llinas M, Ulrich EL, Markley JL, Ionides J and Laue ED (2005) The CCPN data model for NMR spectroscopy: development of a software pipeline. *Proteins* **59**(4): 687-696.

Xiao Y, Bingham JP, Zhu W, Moczydlowski E, Liang S and Cummins TR (2008) Tarantula Huwentoxin-IV inhibits neuronal sodium channels by binding to receptor site 4 and trapping the domain II voltage sensor in the closed configuration. *J Biol Chem* **283**(40): 27300-27313.

Yang Y, Wang Y, Li S, Xu Z, Li H, Ma L, Fan J, Bu D, Liu B, Fan Z, Wu G, Jin J, Ding B, Zhu X and Shen Y (2004) Mutations in *SCN9A*, encoding a sodium channel alpha subunit, in patients with primary erythermalgia. *J Med Genet* **41**(3): 171-174.

Footnotes

This research was supported by a National Health and Medical Research Council Project grant [1034958] and an Australia Research Council Future Fellowship [FTl10100925].

J.K.K and Y.K.Y.C contributed equally to this work.

Molecular Pharmacology Fast Forward. Published on October 1, 2015 as DOI: 10.1124/mol.115.100784
This article has not been copyedited and formatted. The final version may differ from this version.

Figure legends

Figure 1. Sequence alignment of peptides in NaSpTx Family 1. '$Na_V1.7$ inhibitor' is defined as a venom-peptide with IC_{50} < 500 nM at $Na_V1.7$ (a)(Li et al., 2003), (b)(Revell et al., 2013), (c)(Bosmans et al., 2006) (effect on $Na_V1.7$ subtype; unpublished data in-house), (d)(Liu et al., 2012) (e)(Klint et al., 2015). Sequence numbering is with respect to Hhn2b. Residues known to be important for inhibition are coloured in dark purple and the fully conserved serine residue (asparagine in Hhn2b) is coloured in pink.

Figure 2. Effect of wild-type Hhn2b and mutants on $hNa_V1.7$ in CHO cells. (A) Representative sodium currents before (black) and after addition of 1 μM (red) or 10 μM (green) of Hhn2b or mutants. Currents were evoked by depolarization to 0 mV from –120 mV. (B) Fraction of inhibition of sodium currents caused by 1 μM of Hhn2b and mutants. Fraction of inhibition was as follows; G7W 0.74 ± 0.01 N24S 0.79 ± 0.08, G7W/N24S 0.28 ± 0.05, G7W/N24A 0.86 ± 0.08, G7W/N24S/W29F 0.56 ± 0.05. The double mutant (G7W/N24S) showed significantly increased inhibition at 1 μM compared to either of the G7W or N24S mutation alone ($P<0.0001$). (C) Inhibition of sodium current as a function of Hhn2b concentration and the two most active mutants. The IC_{50} of the most potent mutants was determined to be 440 ± 4 nM for G7W/N24S and 1.0 ± 0.2 μM (n = 3–6 for each data point; error bars represent s.e.m.). All data was recorded using automated patch-clamp (QPatch^{TM}).

Figure 3. Structure of WT and G7W/N24S mutant of Hhn2b. (A) Cartoon representation of the ensemble of 20 WT (left) and G7W/N24S mutant (right) Hhn2b structures. Hydrophobic residues that make up the hydrophobic face are shown in

sticks and the site of mutations are highlighted in orange. (B) Surface of peptides with the hydrophobic residues highlighted in green and the residues that bear a positively charged side chain highlighted in blue. (C) Overlay of the WT (green) and the G7W/N24S mutant (purple) structure. PDB ID for the WT and G7W/N24S Hhn2b are 2MQF and 2MXO, respectively.

Figure 4. Chemical shift difference between WT and G7W/N24S mutant of Hhn2b. The bar charts show the absolute difference of all ^{1}H (top), ^{13}C (middle) and ^{15}N (bottom) chemical shifts between the WT and the G7W/N24S mutant for each residue.

Figure 5. NH region of 1D ^{1}H-NMR spectra of Hhn2b (WT) and mutants in the presence of excess amount of POPG liposomes. In the presence of POPG the spectra of WT and N24S mutants remain well resolved containing well dispersed sharp lines, comparable to the spectra measured in the absence of liposomes. In contrast to this almost all signals from the G7W mutant and G7W/N24S double mutant were severely broadened, indicative of binding of the peptide to the liposomes. In all experiments the peptide:POPG ratio was 1:30.

Molecular Pharmacology Fast Forward. Published on October 1, 2015 as DOI: 10.1124/mol.115.100784
This article has not been copyedited and formatted. The final version may differ from this version.

Tables

Table 1. Tested mutants of Hhn2b with indication of the mutated residue, the IC_{50} value obtained by automated patch-clamp, the hill slope for the fit of the curve and the number of repeats for each determined curve.

Peptide	Amino acid sequence	IC50 (µM)	Hill slope	n
Hhn2b	AECKGFGKSCVPGKNECCSGYACNSRDKWCKVLL	> 10	-	6
Hhn2b-K4L	AEC**L**GFGKSCVPGKNECCSGYACNSRDKWCKVLL	> 10	-	3
Hhn2b-G7W	AECKGF**W**KSCVPGKNECCSGYACNSRDKWCKVLL	2.7 ± 0.4	1.5 ± 0.5	5
Hhn2b-N24S	AECKGFGKSCVPGKNECCSGYAC**S**SRDKWCKVLL	4.0 ± 0.5	1.3 ± 0.2	4
Hhn2b-V32W	AECKGFGKSCVPGKNECCSGYACNSRDKWCK**W**LL	> 10	-	4
Hhn2b-G7W/N24A	AECKGF**W**KSCVPGKNECCSGYAC**A**SRDKWCKVLL	8.6 ± 1.7	1.4 ± 0.4	6
Hhn2b-G7W/N24S	AECKGF**W**KSCVPGKNECCSGYAC**S**SRDKWCKVLL	0.44 ± 0.04	1.3 ± 0.1	5
Hhn2b-G7W/N24S/W29A	AECKGF**W**KSCVPGKNECCSGYAC**S**SRDK**A**CKVLL	> 10	-	6
Hhn2b-G7W/N24S/W29F	AECKGF**W**KSCVPGKNECCSGYAC**S**SRDK**F**CKVLL	1.0 ± 0.2	1.0 ± 0.2	4

Molecular Pharmacology Fast Forward. Published on October 1, 2015 as DOI: 10.1124/mol.115.100784
This article has not been copyedited and formatted. The final version may differ from this version.

Table 2. NMR and refinement statistics for 20 structures of WT and G7W/N24S mutant of Hhn2b peptide. Sterochemical quality according to MolProbity (http://helix.research.duhs.duke.edu). Clashscore is the number of steric overlaps >0.4 Å per 10^3 atoms. All statistics are given as mean ± standard deviaiton.

	Hhn2b WT	Hhn2b G7W/N24S
PDB ID	2MQF	2MXO
Experimental restraints		
Inter-proton distance restraints		
Total	446	437
Intra-residue ($i = j$)	125	141
Sequential ($\|i - j\| = 1$)	124	128
Medium range ($1 < \|i – j\| < 5$)	60	63
Long range ($\|i – j\| \geq 5$)	137	105
Disulfide bond restraints	9	9
Dihedral-angle restraints (ϕ, ψ)	55	50
Total number of restraints per residue	15	14.6
RMSD to mean coordinate structure, Å		
Backbone atoms	0.34 ± 0.10	0.40 ± 0.14
All heavy atoms	0.77 ± 0.11	1.3 ± 0.24
Backbone atoms (Residues 3–32)	0.17 ± 0.05	0.14± 0.04
Heavy atoms (Residues 3–32)	0.63 ± 0.13	1.18 ± 0.27
Stereochemical quality		
Ramachandran plot statistics		
Most favored region, %	95.3 ± 3.44	93.0 ± 2.66
Disallowed regions, %	0 ± 0	0 ± 0
Unfavorable sidechain rotamers, %	3.65 ± 1.42	4.95 ± 1.23
Clashscore, all atoms	0 ± 0	0 ± 0
Overall MolProbity score (percentile)	91.5 ± 4.17	82.7 ± 5.09

Molecular Pharmacology Fast Forward. Published on October 1, 2015 as DOI: 10.1124/mol.115.100784
This article has not been copyedited and formatted. The final version may differ from this version.

Figure 1

Molecular Pharmacology Fast Forward. Published on October 1, 2015 as DOI: 10.1124/mol.115.100784
This article has not been copyedited and formatted. The final version may differ from this version.

Figure 2

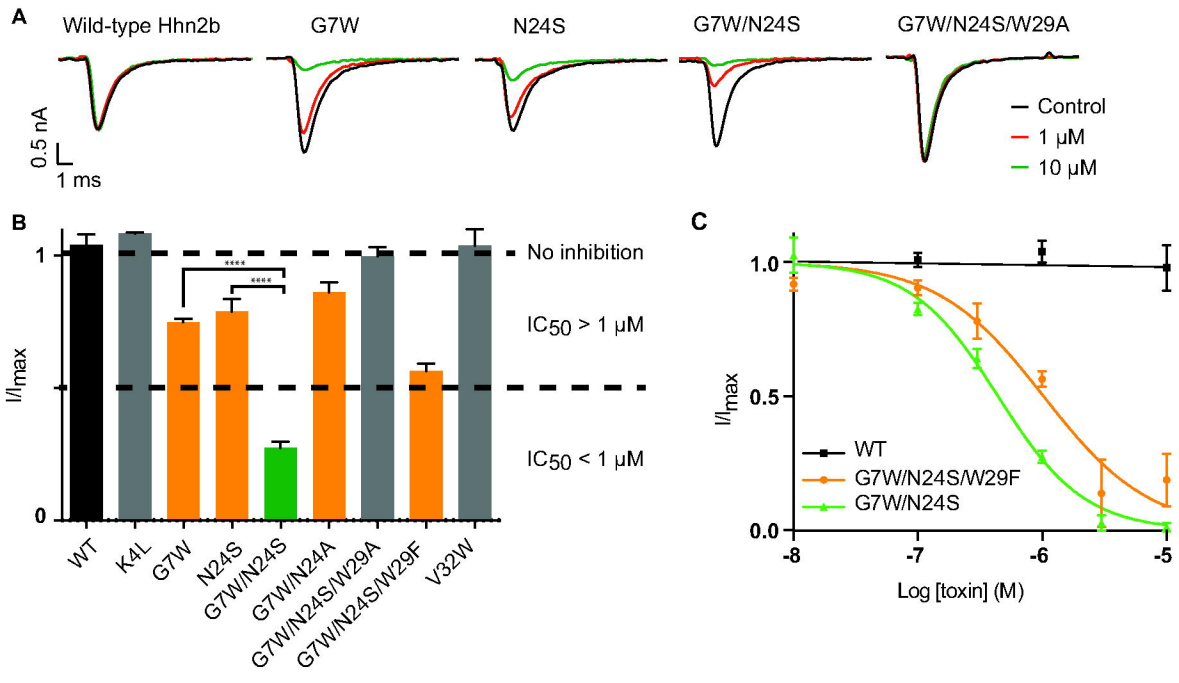

Figure 3

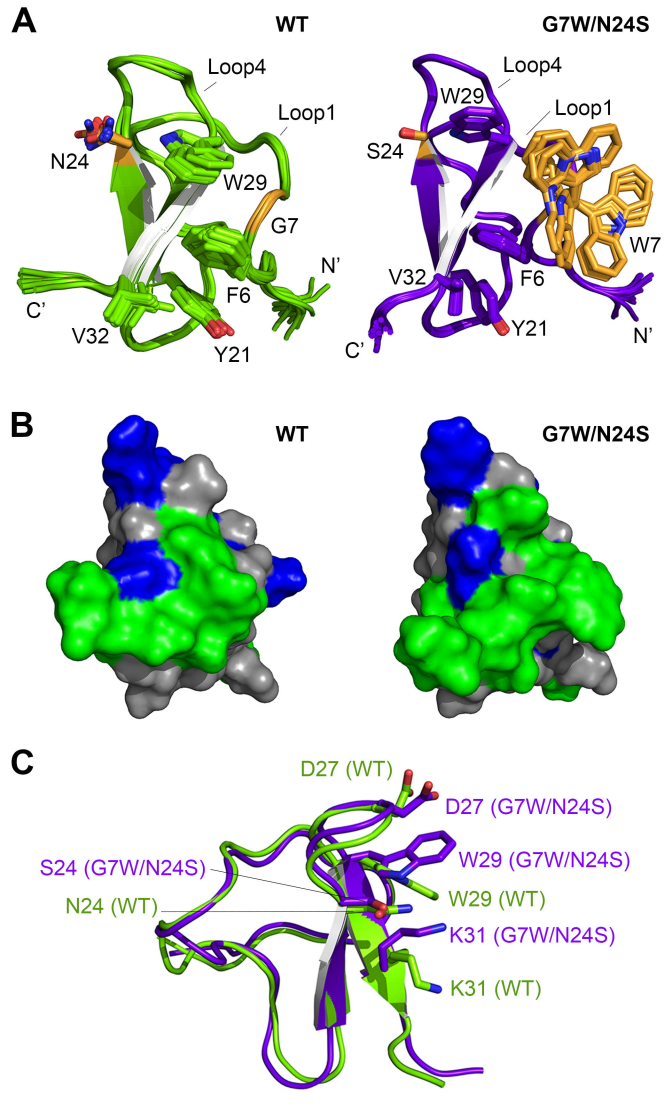
A
WT
G7W/N24S
Loop4
Loop1
N24
W29
G7
N'
C'
F6
V32
Y21
S24
W7
B
C
D27 (WT)
D27 (G7W/N24S)
S24 (G7W/N24S)
W29 (G7W/N24S)
N24 (WT)
W29 (WT)
K31 (G7W/N24S)
K31 (WT)

Molecular Pharmacology Fast Forward. Published on October 1, 2015 as DOI: 10.1124/mol.115.100784
This article has not been copyedited and formatted. The final version may differ from this version.

Figure 4

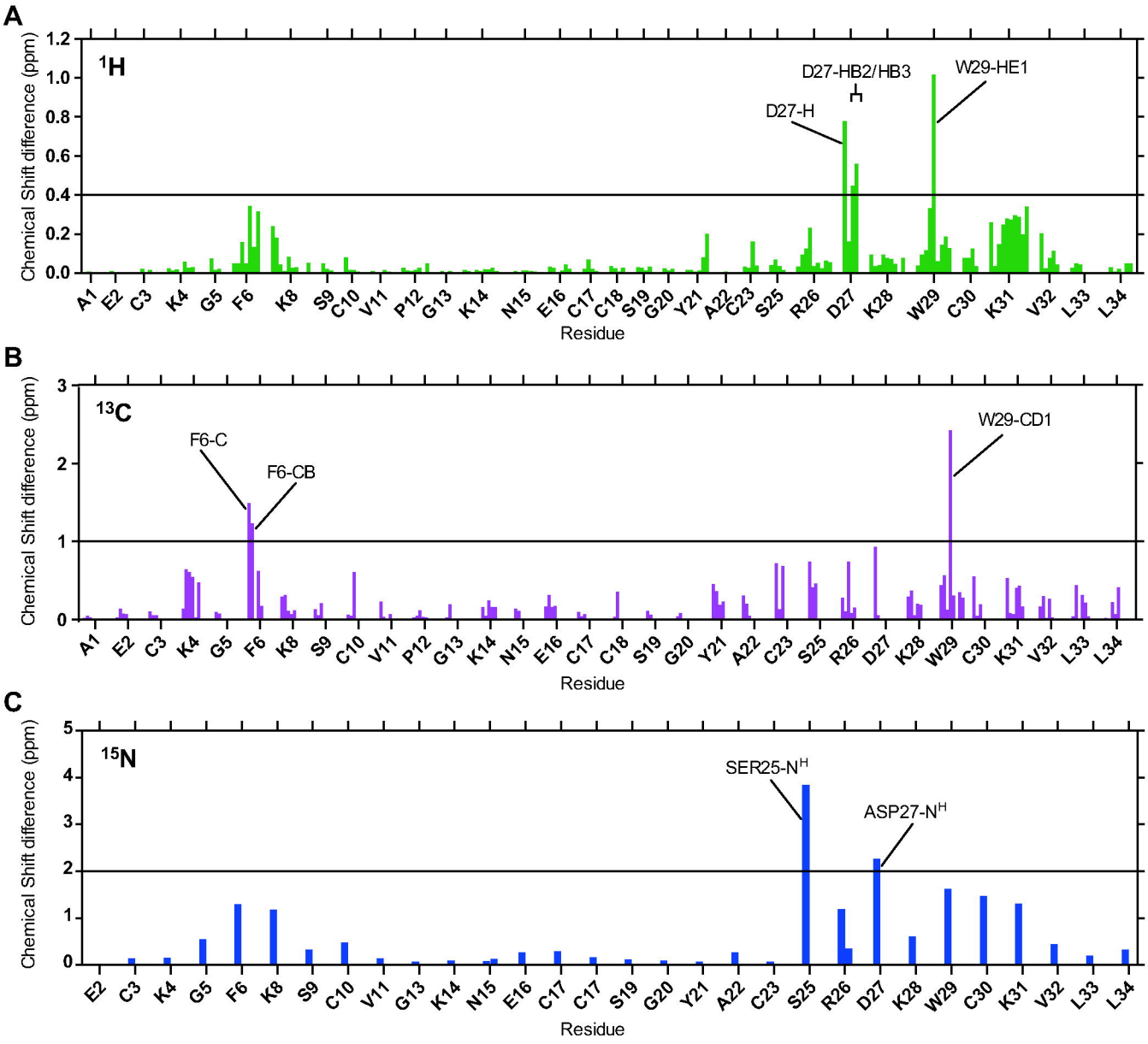

Molecular Pharmacology Fast Forward. Published on October 1, 2015 as DOI: 10.1124/mol.115.100784
This article has not been copyedited and formatted. The final version may differ from this version.

Figure 5

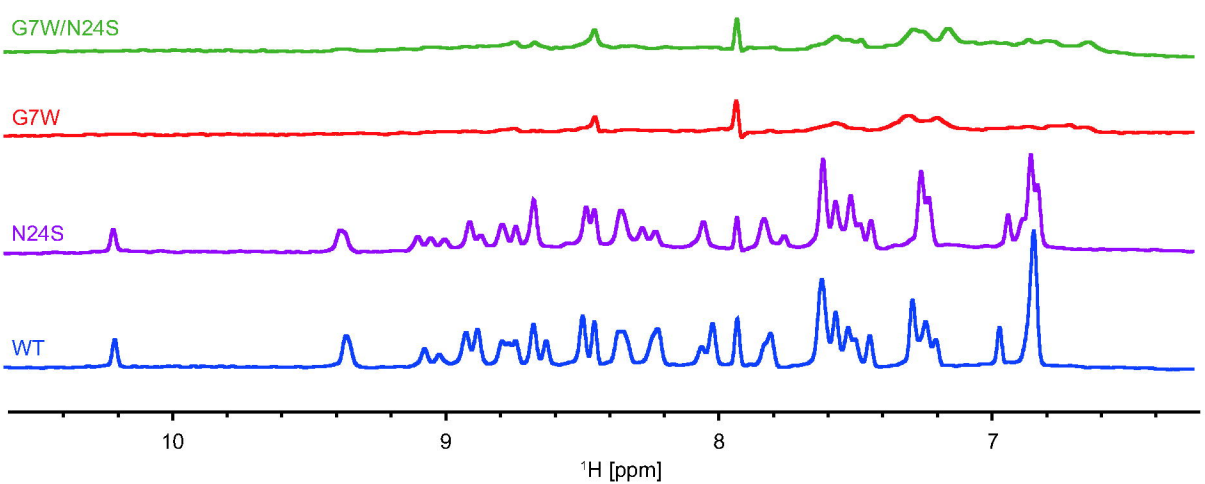

Molecular Pharmacology

Supplemental Data

Rational engineering defines a molecular switch that is essential for activity of spider-venom peptides against the analgesics target $Na_V1.7$

Julie K. Klint, Yanni K.-Y. Chin, and Mehdi Mobli

Institute for Molecular Bioscience, The University of Queensland, St. Lucia, QLD 4072, Australia (J.K.K., Y.K.Y.C); Centre for Advanced Imaging, The University of Queensland, St. Lucia, QLD 4072, Australia (M.M)

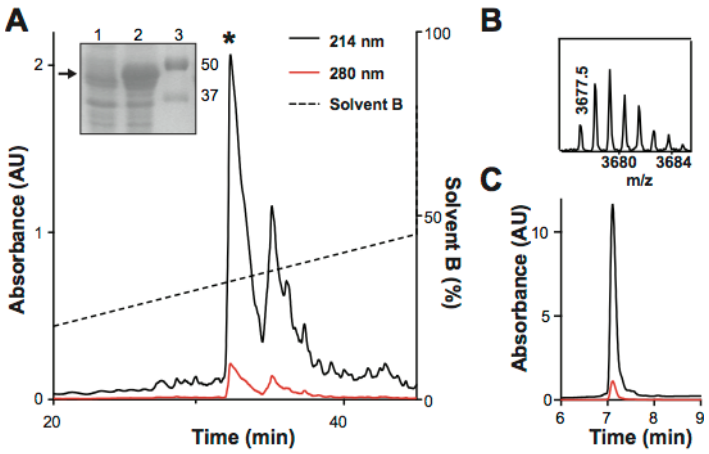

Supplemental Fig. S1. Expression and purification of wild-type Hhn2b. (A) RP-HPLC chromatogram showing purification of recombinant Hhn2b after removal of the His_6-MBP fusion tag by TEV protease. The peak corresponding to Hhn2b is highlighted with an asterisk. Inset, SDS-PAGE gel showing *E. coli* cells before (lane 1) and after (lane 2) IPTG induction. Lane 3 contains molecular mass standards, with masses indicated in kDa on the right of the gel. The arrow indicates the position of the MBP-peptide fusion protein. (B) MALDI-TOF MS spectrum showing the $M+H^+$ ion for the purified fully oxidized recombinant Hhn2b: observed 3677.5 Da, calculated 3677.7 Da. (C) RP-HPLC chromatogram of purified Hhn2b showing high purity as judged by one single uniform peak.

Figure S2

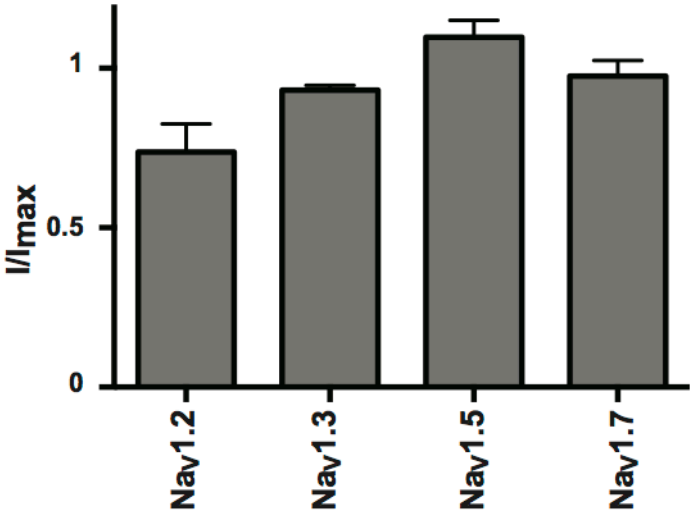

Supplemental Fig. S2. Wild-type recombinant Hhn2b has no or little effect on human Na_V channels. Currents were recorded from channels heterologously expressed in *X. laevis* oocytes using two-electrode voltage-clamp. I/I_{max} in the presence of 1 μM of Hhn2b (*n* = 3–4; error bars represent s.e.m.). Hhn2b had no effect on human $Na_V1.3$, $Na_V1.5$ or $Na_V1.7$, and gave 25% inhibition of $Na_V1.2$. Currents were evoked by depolarization to –20 mV from a holding potential of –90 mV. All channels were co-expressed with the β1 subunit.

Figure S3

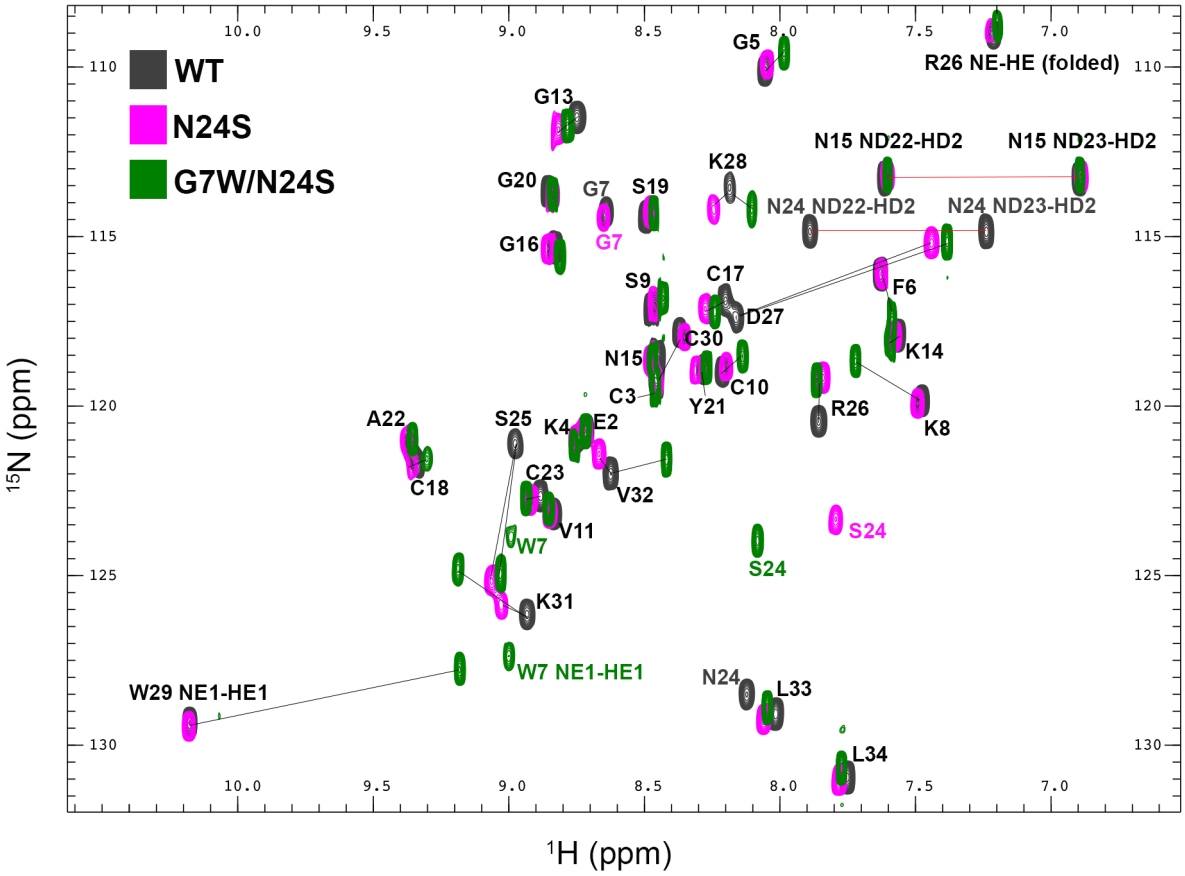

Supplemental Fig. S3. **Overlay of the 2D ^{1}H-^{15}N-HSQC spectra of WT, N24S and G7W/N24S mutants of Hhn2b.** Spectra are shown in grey, magenta and green for the WT, N24S and G7W/N24S mutants, respectively. Red lines connect the two peaks corresponding to the sidechain amide group of Asn15/24 and black lines connect peaks that have shifted upon the mutations.

Figure S4

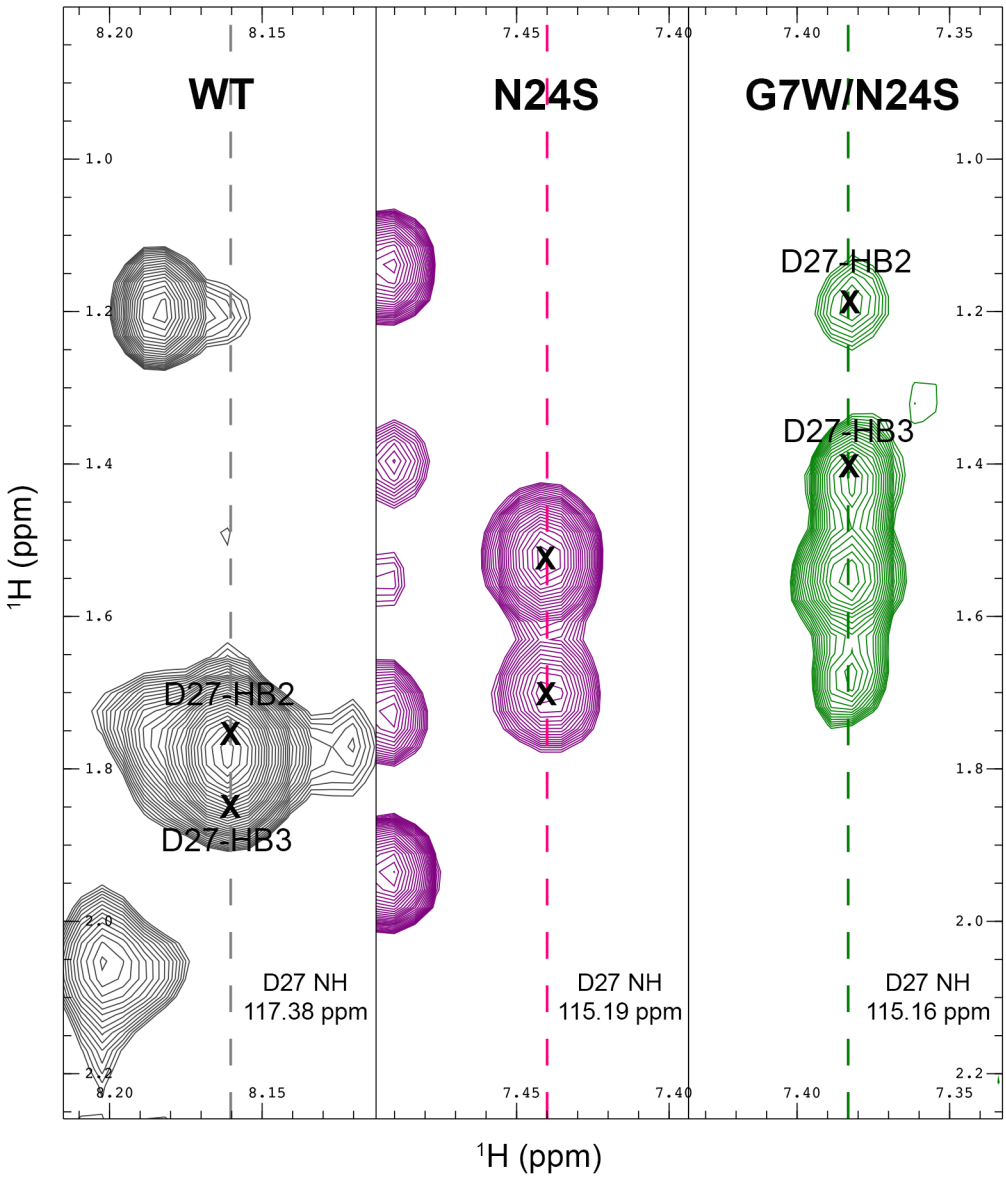

Supplemental Fig. S4. ^{15}N-NOESY strips showing the intramolecular NOE signals of the β-protons of Asp27 in WT, N24S and G7W/N24S mutants of Hhn2b. The signals of the D27 sidechain protons are consistently shifted to lower frequencies as the two mutations are introduced, indicating increased proximity to an aromatic ring.

Figure S5

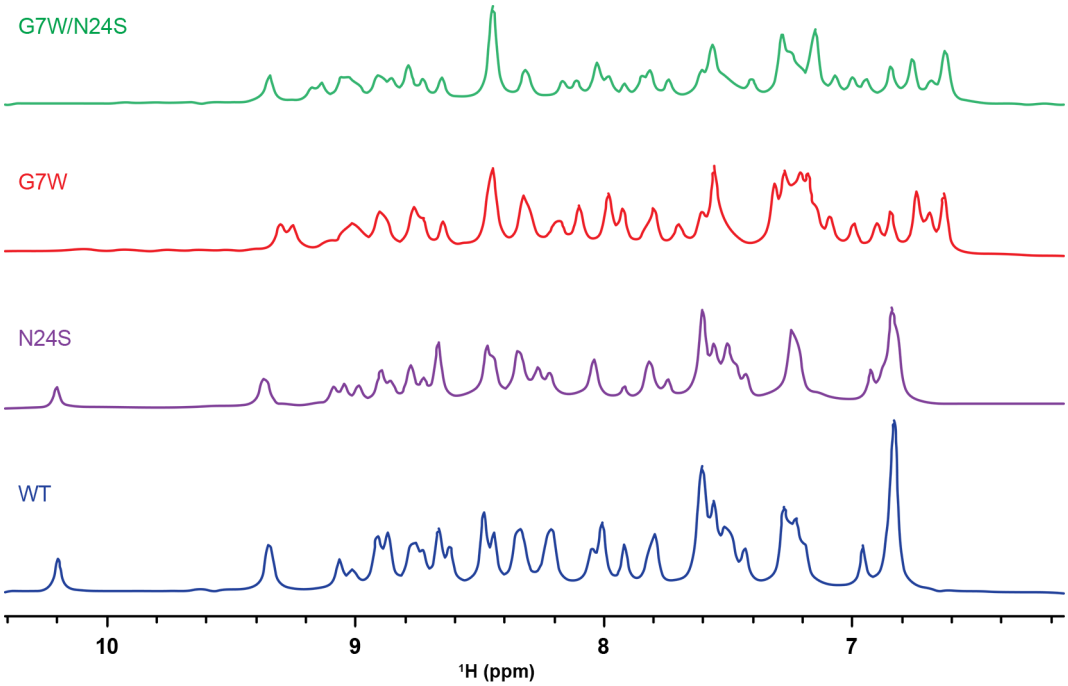

Supplemental Fig. 5. NH region of 1D ^{1}H-NMR spectra of Hhn2b (WT) and mutants in the presence of excess amount of POPC liposomes. In the presence of POPC the spectra of all Hhn2b and mutants remain well resolved. In all experiments the peptide:POPC ratio was 1:30.